nanomaterials

MDPI

Article

Distinguishing the Charge Trapping Centers in CaF_2-Based 2D Material MOSFETs

Zhe Zhao [1,2], Tao Xiong [2], Jian Gong [1,3,*] and Yue-Yang Liu [2,*]

[1] School of Physical Science and Technology, Inner Mongolia University, Hohhot 010021, China; zhezhao@mail.imu.edu.cn
[2] State Key Laboratory of Superlattices and Microstructures, Institute of Semiconductors, Chinese Academy of Sciences, Beijing 100083, China; xiongtao@semi.ac.cn
[3] Ordos Institute of Technology, Ordos 017000, China
* Correspondence: ndgong@imu.edu.cn (J.G.); yueyangliu@semi.ac.cn (Y.-Y.L.)

Abstract: Crystalline calcium fluoride (CaF_2) is drawing significant attention due to its great potential of being the gate dielectric of two-dimensional (2D) material MOSFETs. It is deemed to be superior to boron nitride and traditional silicon dioxide (SiO_2) because of its larger dielectric constant, wider band gap, and lower defect density. Nevertheless, the CaF_2-based MOSFETs fabricated in the experiment still present notable reliability issues, and the underlying reason remains unclear. Here, we studied the various intrinsic defects and adsorbates in CaF_2/molybdenum disulfide (MoS_2) and CaF_2/molybdenum disilicon tetranitride ($MoSi_2N_4$) interface systems to reveal the most active charge-trapping centers in CaF_2-based 2D material MOSFETs. An elaborate Table comparing the importance of different defects in both n-type and p-type devices is provided. Most impressively, the oxygen molecules (O_2) adsorbed at the interface or surface, which are inevitable in experiments, are as active as the intrinsic defects in channel materials, and they can even change the $MoSi_2N_4$ to p-type spontaneously. These results mean that it is necessary to develop a high-vacuum packaging process, as well as prepare high-quality 2D materials for better device performance.

Keywords: CaF_2; 2D material MOSFETs; reliability; charge trapping

Citation: Zhao, Z.; Xiong, T.; Gong, J.; Liu, Y.-Y. Distinguishing the Charge Trapping Centers in CaF_2-Based 2D Material MOSFETs. *Nanomaterials* **2024**, *14*, 1038. https://doi.org/10.3390/nano14121038

Academic Editor: Arthur P. Baddorf

Received: 24 April 2024
Revised: 1 June 2024
Accepted: 11 June 2024
Published: 16 June 2024

1. Introduction

Two-dimensional (2D) materials offer new possibilities for advancing Moore's Law due to their ultra-thin thickness and smooth surface with no dangling bonds [1–9]. The ultra-scaled channel places higher demands on the quality and reliability of gate dielectric materials. However, common oxides (such as SiO_2 [10], hafnium dioxide (HfO_2) [11], and aluminum trioxide (Al_2O_3) [12]) that are used in silicon technologies are non-layered, which makes it difficult for them to form a good interface with 2D channels. To deal with the problem, 2D dielectrics such as hexagonal boron nitride (h-BN) have been studied [13]. However, the band gap (~6 eV) and dielectric constant (5.06 ε) of h-BN are not satisfying for dielectric materials [14]. Its band offset with 2D materials is not large enough, which will lead to many reliability problems [15].

Recent experimental preparation of crystalline CaF_2 provides a promising solution to the dilemma [16,17]. By using molecular beam epitaxy (MBE), crystalline CaF_2 can be grown on a silicon or germanium substrate [18]. It has a larger bandgap (12.1 eV) and dielectric constant (8.43 ε) than h-BN [19]. The grown CaF_2 is terminated by F atoms, which means that there are no dangling bond on its surface [20]. At the same time, wafer-scale CaF_2 was prepared by the magnetron sputtering method as a substrate for optoelectronic devices, resulting in the formation of good van der Waals devices with Tin disulfide (SnS_2) and Tungsten disulfide (WS_2). The electronic mobility and photoresponsivity of the devices were improved by an order of magnitude higher compared to SiO_2-based devices [21]. Another important point is that CaF_2 itself is stable in air, and is not easily dissolved in water [22]. CaF_2 can form good I-band alignment with many 2D materials, such as silicon carbide (SiC). The valence band offset of 2D SiC/CaF_2 is as high as 3.5 eV, and even if there are carbon antisite and interstitial defects on the 2D SiC surface, it will not affect CaF_2 [23]. This means that it will be very advantageous as a gate dielectric for semiconductor devices.

Nevertheless, notable device reliability issues were still observed in CaF_2-based MOSFETs [19,22,24,25], which contradicts the perfect electrical properties of CaF_2. For example, the I_D-V_G hysteresis is significant (although, lower than that in MoS_2/SiO_2 FET), and it shows obvious variability when the same device is operated at different scanning times. On the other hand, when different devices are operated under the same V_D, the I_D-V_G characteristics such as on/off current ratio and subthreshold swing (SS) (150–90 mV dec^{-1}) differ greatly [19]. In addition, some devices with large negative threshold voltage (V_{th}) are prone to fail due to the bias overload of the CaF_2 layer. The physical origin of hysteresis and threshold voltage shift is widely attributed to the charge trapping and de-trapping of microscopic defects [26–32], and the strength of the charge trapping effect is closely related to the type of defects [33–36]. In graphene/CaF_2 FETs, the hysteresis and bias–temperature instabilities (BTI) phenomenon are both observed due to the presence of defects. They are not detrimental to device performance due to the intrinsic advantage of CaF_2, but the problem cannot be avoided [37]. The hysteresis is also observed in ReS_2 FETs, and it is subjected to variations in temperature, sweeping gate voltage, and pressure during experiments, demonstrating the existence of a charge-trapping and de-trapping effect [38].

The presence of trapping centers at the interface not only affects the reliability of transistors, but also has an impact on other kinds of semiconductor devices, such as thermoelectric devices composed of tin dioxide (SnO_2) [39] and solar cell devices composed of perovskite materials such as perovskite solar cells (PSCs) [40]. Therefore, distinguishing active trapping centers, and then finding ways to eliminate them, is crucial for the improvement of semiconductor devices. Unfortunately, it is difficult to determine the specific contribution of each kind of defect to the charge-trapping process through experiments. Under such circumstances, we decides to use principles calculations to distinguish the active charge-trapping centers in CaF_2-based 2D MOSFETs first, and then provide guidance to experimental researchers to analyze and improve the performance and reliability of their devices.

In this work, realistic MoS_2/CaF_2 and $MoSi_2N_4/CaF_2$ interface models have been constructed to study the charge-trapping centers in various positions. CaF_2 is designed as a 5-layer structure, which is consistent with the experimental report [19,41]. The fabricated device in the experiment contains a 2-layer MoS_2 and a 2 nm thick CaF_2, which is 5 layers. At the same time, 13 types of defects were systematically investigated, and several positions for each type of defect were studied to avoid randomness. When analyzing defects, we not only considered the defect energy levels, but also the defect formation energy and their importance in n-type and p-type transistors, respectively. To ensure the accuracy of the data, Heyd–Scuseria–Ernzerhof (HSE) hybrid functionals were used, even though they require a large amount of computing resources.

2. Materials and Methods

Among the 2D materials, MoS_2 is one of the most widely used semiconductors [42–45]. It has a direct band gap of 1.8 eV, and has been used to design high-performance electronic and optoelectronic devices [5]. On the other hand, there are also some new materials being synthetized, such as the $MoSi_2N_4$ [46]. $MoSi_2N_4$ is very promising because of the excellent photocatalytic performance [47], mechanical strength [48], and electrical transportability [49]. Therefore, we construct both MoS_2/CaF_2 and $MoSi_2N_4/CaF_2$ interface models to make the simulation results representative. The lattice parameter of CaF_2, MoS_2, and $MoSi_2N_4$ is 3.90 Å, 3.16 Å, and 2.91 Å, respectively. To achieve good lattice matching, the primary cell of MoS_2 is repeated five times to contact the CaF_2 cell, which is repeated four times. The final CaF_2 deformation is only 1.28%. Similarly, the primary cell of $MoSi_2N_4$

is repeated four times to contact the CaF_2, while the CaF_2 deformation is repeated three times and is only 0.52%.

To make the results reliable, different types of defects/impurities, not only within the material, but also at the interfaces and surfaces, were studied. For CaF_2, even though previous studies have shown that it only contains a very small number of F defects (V_F), for the sake of data reliability, research was still conducted on V_F defects. Meanwhile, our research found that V_F contributes two electrons to CBM, which had not been discovered by previous researchers. For MoS_2, we considered S vacancy defect (V_S), Mo vacancy defects (V_{Mo}), MoS_3 vacancy defect (V_{MoS3}) and MoS_6 vacancy defect (V_{MoS6}) at different spatial locations. MoS_2 is composed of one Mo atom in the middle and three S atoms on the upper and lower surfaces. A MoS_3 defect is defined as the loss of a Mo atom and three S atoms connected to it, either in the upper or lower layers. The MoS_6 defect is formed by the loss of both the Mo atom in the middle and the six S atoms connected to it. On the other hand, considering that gas adsorption is occurs very easily in the process of device manufacturing, we also studied the water and oxygen molecules that adsorbed at different positions. For a more intuitive display of defects and adsorption, the related structural diagrams are shown in following figures. For $MoSi_2N_4$, both its N vacancies (V_N) and Si vacancies (V_N) were studied simultaneously. Same as MoS_2, gas adsorption in $MoSi_2N_4$ during preparation is also a factor that may affect device stability. The adsorption of O_2 and water molecules (H_2O) was studied in CaF_2-$MoSi_2N_4$.

All the first-principles calculations were performed by the software PWmat [50,51]. The SG15 pseudopotential [52] was adopted, and the plane wave cutoff energy was 50 Ry. The Perdew–Burke–Ernzerhof (PBE) functional was used for structural relaxation with a convergence criterion of 10^{-5} eV/Å. The HSE [53] functional was used in the calculation of electronic structures to improve the accuracy of calculations. All calculations were performed using gamma points (0,0,0) considering the largeness of the supercells, and this is a common strategy to deal with large models [34,35]. VdW-D3 was used to correct the interlayer interaction of the material. The DFT-D3 energy formula is as follows: $E_{DFT-D3} = E_{KS-DFT} - E_{disp}$, E_{KS-DFT} is the usual self-consistent KS energy and E_{disp} is the dispersion correction as a sum of two- and three-body energies [54]. The equilibrium distance between the MoS_2 and CaF_2 and between the CaF_2 and $MoSi_2N_4$ was 2.89 Å and 2.93 Å, respectively. For MoS_2, the impact of point defects on the equilibrium distance was not significant, only 1.04%. For larger defects, there may have been some impacts, among which V_{MoS3} decreased the distance by 8.65% to 2.64 Å. O_2 adsorption resulted in an equilibrium distance of 3.03 Å, which represented an increase of 5.21%. For $MoSi_2N_4$, the V_N defect showed a change in the equilibrium distance between CaF_2-$MoSi_2N_4$, with an equilibrium position of 2.72 Å, representing a 7.17% decrease. H_2O adsorption resulted in an equilibrium position of 3.10 Å, which represented an increase of 5.80%. The data above show that defects and adsorption can slightly change the equilibrium distance between interfaces, but their impact is not significant. All the calculation processes are shown in Figure 1.

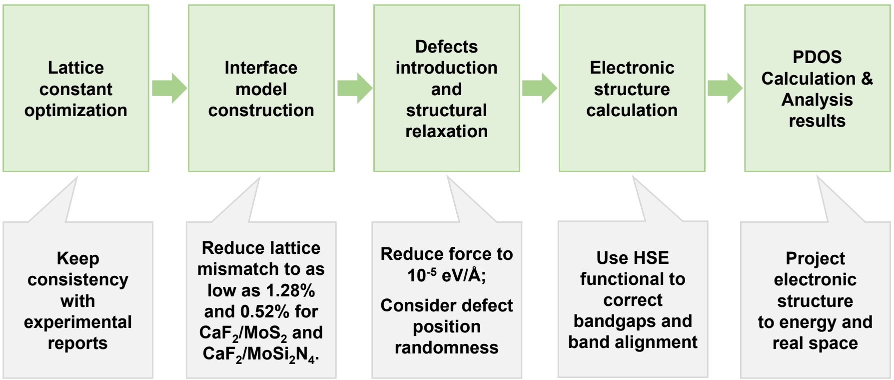

Figure 1. Flowchart of calculation method.

3. Results

3.1. The Charge-Trapping Centers in CaF_2-MoS_2

The CaF_2-MoS_2 interface models are shown in Figure 2a. Blue, gray, purple, yellow, white, and red spheres are used in the figure to represent Ca, F, Mo, S, H, and O atoms. Figure 2a shows the adsorption and defects (green spheres) present at different interfaces and surfaces of CaF_2-MoS_2. A 5-layer CaF_2 is adopted because the experimental MBE grown CaF_2 is about 2 nm thick. The band alignments that manifested by the projected density of states (PDOS) are shown in Figure 2b. The red part in the figure represents the data of DOS, and the depth of the color represents the size of PDOS values. It can be seen that the VBM (valence band maximum) and CBM (conduction band minimum) are provided by MoS_2, and the band offsets are greater than 2 eV, which makes charge tunneling difficult. All Fermi energy levels have been reset to zero, indicated by a green dotted line in the graph. The defect energy level and band offset have a direct impact on the charge-trapping activity. Although the vacuum levels were not adjusted, this does not affect the conclusions reached. This confirms that using CaF_2 as the gate of 2D material MOSFETs is likely to obtain good device reliability [41]. Therefore, when considering practical applications, we believe that the reliability issues should stem from some intrinsic or external charge-trapping centers.

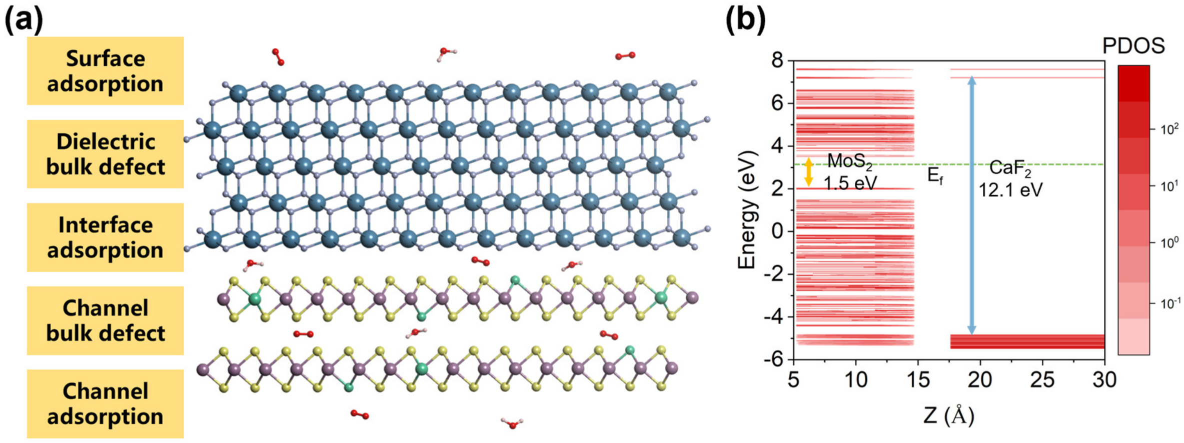

Figure 2. Atomic structure and type-I band alignment of CaF_2-MoS_2 interface models. (**a**) Atomic structure of 5-layer CaF_2 and 2-layer MoS_2, as well as (**b**) band alignment along the *Z*-axis direction.

3.1.1. The Charge-Trapping Centers in CaF_2

Intuitively, we should first study the F vacancy defect in the CaF_2 layer. However, it has been demonstrated in experiments that generating defects in CaF_2 is not easy [19]. Furthermore, it has been proven by a first-principle calculation that even though F vacancies (V_F) and Ca vacancies (V_{Ga}) exist, there is no defect state near the band edge of channel material due to the large band offset between the two materials [55]. Nevertheless, to make the conclusion more rigorous, we still conducted relevant calculations on the V_F. In Figure 3, the energy levels of CaF_2, MoS_2, and V_F are represented by green, blue, and red, respectively. In the calculation, both vdW and electron spin are considered, and the randomness of V_F positions is also taken into account. For ease of observation, the PDOS value of V_F in Figure 3 has been expanded 50 times. As the focus is on the defect energy level of V_F, it does not affect the results. The band alignment of CaF_2 and MoS_2 here is consistent with Figure 2b, and MoS_2 provides VBM and CBM. The offset between the V_F defect energy level and CBM is 4.43 eV, indicating that even with defects, it is not easy to trap charges. Consequently, we turn our attention to the trapping centers inside the channel material, in the semiconductor/dielectric interface, and at the dielectric surface.

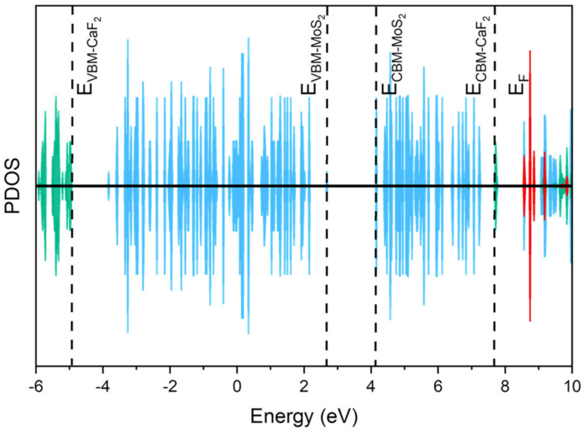

Figure 3. The position of the F vacancy (V_F) defect energy level in the CaF_2 band. The blue, green, and red lines represent the PDOS of CaF_2, MoS_2, and V_F, respectively.

3.1.2. The Charge-Trapping Centers in the Channel

The energy level distribution of different defects in MoS_2 is shown in Figure 4. First, in Figure 4a, there is an occupied defect state denoted by d1 for the vs. in MoS_2, whose energy is 0.38 eV below VBM, and there are two empty defect states with similar energy denoted by d2, whose energy is 0.57 eV below CBM. According to charge transfer theories, the charge-trapping rate will decrease exponentially with the increasing energy barrier between the initial and final electronic states; thus, we can consider that only the defect levels located less than 1 eV away from the MoS_2 band edge are active trapping centers. Therefore, it can be concluded that d1 is an important hole-trapping state in p-FETs, and d2 is an important electron-trapping state in n-FETs. Similarly, in Figure 4b, the Mo vacancy is active in trapping holes and electrons, but not as active as the S vacancy in electron trapping because the V_{Mo} defect levels are farther away from the CBM. In addition to the common vs. and V_{Mo}, experiments have reported that complex vacancy defects (such as V_{MoS3} and V_{MoS6}, as shown in Figures 4c and 4d, respectively) are found in MoS_2 [56]. These two complex vacancies contain many dangling bonds, and thus, can introduce a series of defect states (up to 13) located either close to VBM or to CBM. Consequently, they will be very active charge-trapping centers. However, the energy of the formation of these complex defects is very high, resulting in a low density. More details of the defect levels have been listed in Table 1.

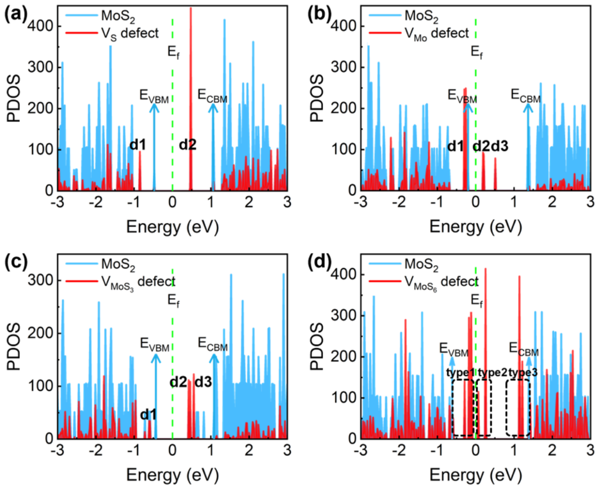

Figure 4. The energy level distribution of different defects. (**a**) S vacancy (V_S), (**b**) Mo vacancy (V_{Mo}), (**c**) MoS_3 vacancy (V_{MoS3}), and (**d**) MoS_6 vacancy (V_{MoS6}).

Table 1. Importance of different trapping centers in CaF_2-MoS_2.

Defect Types	Defect State	ΔE-VBM (eV)	ΔE-CBM (eV)	n-FET Importance	p-FET Importance	Fromation Energy (eV)	Overall Importance
V_S	d1	−0.38	−1.91	✓	✗	2.91	✓
	d2	0.95	−0.57	✓	✓		
V_{Mo}	d1	−0.06	−1.63	✓	✗	8.52	✓
	d2	0.40	−1.17	✗	✓		
	d3	0.71	−0.86	✗	✓		
V_{MoS3}	d1	−0.25	−1.78	✓	✗	11.81	✓
	d2	0.89	−0.64	✗	✓		
	d3	0.99	−0.53	✗	✓		
V_{MoS6}	type1	<0.50	>1.50	✓	✗	21.41	✗
	type2	<1.00	>1.00	✗	✗		
	type3	>1.75	<0.25	✗	✓		
O_2 at interface	d1	−0.99	−2.45	✓	✗	0.68	✓
	d2	−0.55	−2.00	✓	✗		
	d3	−0.85	−2.31	✓	✗		
H_2O at interface		−3.42	−4.91	✗	✗	0.61	✗
O_2 in MoS_2		−0.37	−2.01	✓	✗	2.35	✓
O_2 at surface		1.11	−0.41	✗	✓	2.25	✓

3.1.3. The Charge-Trapping Centers in the Interface and Surface

It has been mentioned in previous reports that the hysteresis of CaF_2-MoS_2 devices can be reduced after they are heated and dried [19]. This indicates that molecules had been adsorbed during device preparation, so the activity of these adsorbates needs to be discussed. Figure 5 shows the adsorption of O_2 at the CaF_2-MoS_2 interface, and three defect levels denoted by d1, d2 and d3 are observed. They are only 1 eV, 0.85 eV and 0.54 eV below VBM, respectively. Therefore, they will be active hole traps in p-MOSFETs. In contrast, the adsorption of water molecules at the interface is much less important because they do not induce obvious defect states near the band edge of MoS_2.

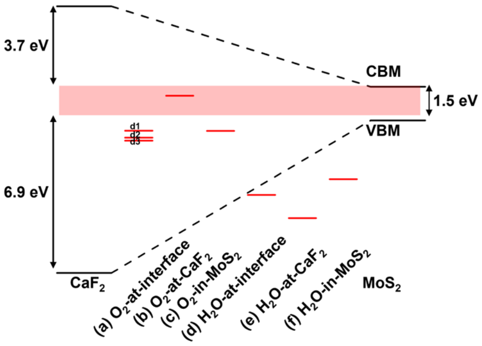

Figure 5. The energy level distribution of different molecules adsorbed on the surface and interface of CaF_2-MoS_2.

In discussing the adsorption of O_2, we first tested different placement methods, including those parallel and perpendicular to the interface, as shown in Figure 6a. To ensure the reliability of our conclusion, we tested O_2 at three different positions, as shown in Figure 6b. The CaF_2 layer was removed from the atomic schematic for ease of observation. Moreover, all of our defects and adsorption structures were tested in at least three different locations to prevent randomness. All results demonstrate the reliability of the existing data. To further check the importance of oxygen, we studied the oxygen that adsorbed in other positions. Figure 5 shows the situation where oxygen molecules are adsorbed in the interlayer of MoS_2. It can be seen that the defect state is only 0.37 eV below VBM, which will trap holes easily, and thus, affects the device performance. Figure 5 shows the case where oxygen is adsorbed on the surface of CaF_2. An occupied defect state that is close to CBM rather than CBM is seen. Considering that the negative gate voltage in a p-FET will drag the defect level down toward the VBM, the oxygen on the CaF_2 surface will form very active hole-trapping centers with large gate voltage.

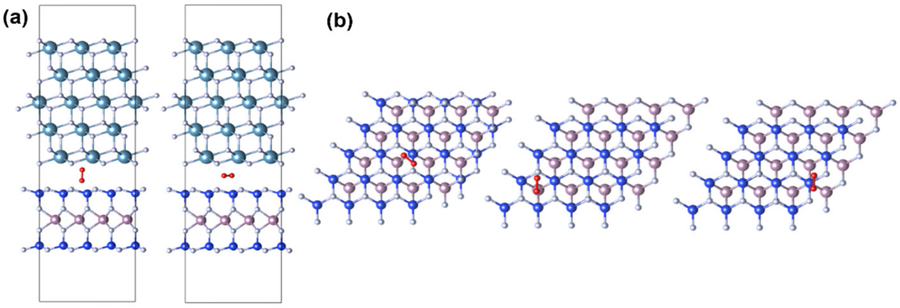

Figure 6. Different situations of O_2 adsorption. (**a**) Compare O_2 perpendicular/parallel to the interface; (**b**) compare different adsorption positions.

To exhibit the importance of different defects more clearly, Table 1 summarizes the information of all defects. The defect levels that are more than 1 eV away from the MoS_2 band edge are regarded as electronically unimportant [57–59]. The $\Delta E_{VBM/CBM}$ is calculated as; moreover, the formation of energy/adsorption energy is considered to provide an overall evaluation of their importance.

3.2. The Charge-Trapping Centers in CaF_2-$MoSi_2N_4$

Now, we study the $MoSi_2N_4$-CaF_2 system. $MoSi_2N_4$ is a 2D material with seven atomic layers. One Mo atomic layer lies in the middle while two Si-N-Si tri-layers lie on the top and bottom surfaces symmetrically. It can be seen that the VBM and CBM are provided by $MoSi_2N_4$ (Figure 7b), and the band offsets are greater than 2 eV, which makes charge tunneling difficult. Vacancy defects caused by the shedding of N atoms and Si (Figure 7a) atoms on the surface layer are the primary problems to be considered. At the same time, the influence of the adsorption of oxygen molecules and water molecules (Figure 7a) during device manufacture is also considered. The atoms highlighted in green in Figure 7a represent defects and adsorption sites.

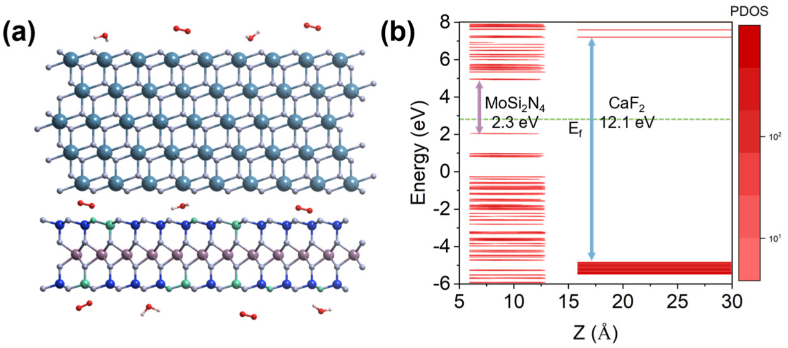

Figure 7. Atomic structure and type-I band alignment of CaF_2-MoS_2 interface models. (**a**,**b**) The atomic structure of 5-layer CaF_2, and 1-layer $MoSi_2N_4$, as well as the band alignment along the *Z*-axis direction.

For the N vacancy (V_N) (Figure 8a), two defect levels are induced into the band gap, of which the half-occupied d1 state is 0.98 eV above VBM and the empty d2 state is 0.45 eV below CBM. Such small energy barriers make them very active hole/electron-trapping centers. In contrast, the V_{Si} defect induces no defect levels close to the CBM, as is shown in Figure 8b, but it induces many defect levels below the VBM. Specifically, the electrons in VBM have spontaneously transferred to the defect sites, shifting the Fermi level below the VBM and making the CaF_2-$MoSi_2N_4$ a whole p-type heterostructure. Interestingly, the adsorption of oxygen in the CaF_2-$MoSi_2N_4$ interface has a very similar effect, as is shown in Figure 8c, the electrons in VBM are spontaneously captured by the oxygen, and the $MoSi_2N_4$ becomes a p-type material. If the oxygen density is high, the performance and reliability of the device will be greatly reduced. In comparison, the adsorption of water molecules in the interface does not have such an effect, as is shown in Figure 8d. The water-related defect energy level is far from the band edge of $MoSi_2N_4$. This further confirms that water molecule adsorption is less important than oxygen adsorption in impacting device performance and reliability. To present the importance of different defects more intuitively, Table 2 summarizes and compares the information of all defects in the CaF_2-$MoSi_2N_4$ system.

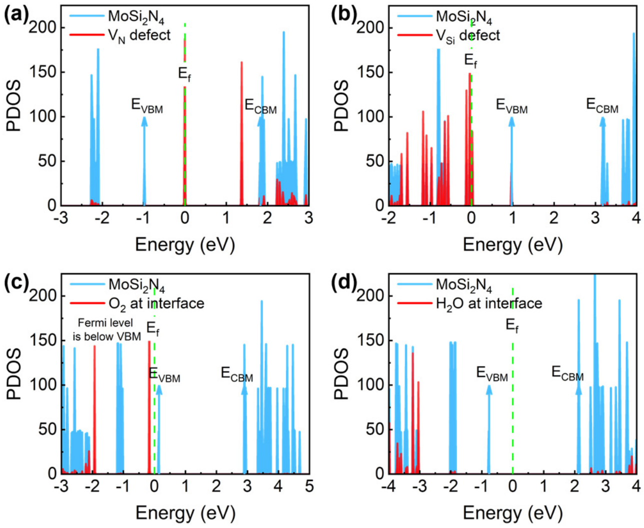

Figure 8. The energy level distribution of different molecules adsorbed on the surface and interface of CaF_2-MoS_2. (**a**) N vacancy (V_N), (**b**) Si vacancy (V_{Si}), (**c**) O_2 at interface, and (**d**) H_2O at interface.

Table 2. Importance of different capture centers in CaF_2-$MoSi_2N_4$.

Defect Types	Defect State	ΔE-VBM (eV)	ΔE-CBM (eV)	n-FET Importance	p-FET Importance	Fromation Energy (eV)	Overall Importance
V_N	d1	0.98	−1.83	✓	✗	5.97	✓
	d2	2.36	−0.45	✗	✓		
V_{Si}	d1	−1.01	−3.23	✗	✗	11.15	✓
	d2	0.00	−2.22	✓	✗		
O_2 at interface		−0.32	−3.07	✓	✗	0.19	✓
H_2O at interface		−2.29	−5.17	✗	✗	0.34	✗

4. Conclusions

In conclusion, we have investigated the various defects and adsorbates in CaF_2-based 2D material MOSFET structures to distinguish their importance in degrading device performance and reliability. First, the intrinsic defects in channel materials, including the Vs. and V_{Mo} in MoS_2, and V_{Si} and V_N in $MoSi_2N_4$, are very active charge-trapping centers. At the same time, although the intrinsic defect V_{MoS6} causes many defect states in the band gap, it is not a significant defect due to its large formation energy. Second, the adsorbed oxygen molecules in the channel/CaF_2 interface or CaF_2 surface are very important trap centers, and they can even spontaneously change the $MoSi_2N_4$ to p-type. Third, the adsorbed water molecules are inactive in capture charges, and thus, are much less important in affecting device performance. An elaborate table comparing the detailed properties of different defects is provided so that both experimental researchers and theorists can refer to it easily. Moreover, the intrinsic defect V_{Si} in CaF_2-$MoSi_2N_4$ can also lead to conversion to p-type transistors. Finally, we found that V_F in CaF_2 spontaneously contributes two electrons to CBM.

The significance of defects or adsorption in CaF_2-based 2D material MOSFETs is not solely contingent upon the defect energy level; rather, it is also contingent upon the formation energy and transport type of the device. The two tables presented in the article provide a comprehensive demonstration of the impact of defects on performance. Furthermore, this methodology can facilitate the development of a system tool in the future, which will enable the determination of the impact of defects on device performance. Especially worth mentioning is the adsorption of oxygen molecules, which is a more problematic phenomenon than the adsorption of water molecules. To avoid this issue, it is advisable to isolate oxygen as much as possible during device preparation or use objects that do not introduce additional pollution sources to adsorb oxygen. These results mean that the exclusion of adsorbates in device fabrication is as important as growing high-quality channel material to obtain better device performance. The findings of our research can be extrapolated to the significance of different capture centers in a variety of 2D material MOSFETs.

Author Contributions: Conceptualization, Z.Z. and Y.-Y.L.; methodology, Z.Z. and Y.-Y.L.; formal analysis, Z.Z., J.G. and Y.-Y.L.; resources, J.G. and Y.-Y.L.; writing—original draft preparation, Z.Z.; writing—review and editing, T.X., J.G. and Y.-Y.L.; funding acquisition, J.G. and Y.-Y.L. All authors have read and agreed to the published version of the manuscript.

Funding: This research was funded by the National Natural Science Foundation of China (Grant No. 62174155 and No. T2293702), CAS Project for Young Scientists in Basic Research (No. YSBR-056), the Inner Mongolia Natural Science Foundation No. 2023ZD27, and the National Natural Science Foundation of China Grant No. 11964022.

Data Availability Statement: The data presented in this study are available on request from the corresponding author.

Acknowledgments: This work acknowledges the support from the School of Physical Science and Technology, Inner Mongolia University and Institute of semiconductors, Chinese Academy of Sciences.

Conflicts of Interest: The authors declare no conflicts of interest.

References

1. Novoselov, K.S.; Geim, A.K.; Morozov, S.V.; Jiang, D.; Zhang, Y.; Dubonos, S.V.; Grigorieva, I.V.; Firsov, A.A. Electric Field Effect in Atomically Thin Carbon Films. *Science* **2004**, *306*, 666–669. [CrossRef] [PubMed]
2. Novoselov, K.S.; Geim, A.K.; Morozov, S.V.; Jiang, D.; Katsnelson, M.I.; Grigorieva, I.V.; Dubonos, S.V.; Firsov, A.A. Two-Dimensional Gas of Massless Dirac Fermions in Graphene. *Nature* **2005**, *438*, 197–200. [CrossRef] [PubMed]
3. Benka, S.G. Two-Dimensional Atomic Crystals. *Proc. Natl. Acad. Sci. USA* **2005**, *102*, 10451–10453. [CrossRef]
4. Geim, A.K.; Novoselov, K.S. The Rise of Graphene. *Nat. Mater.* **2007**, *6*, 183–191. [CrossRef] [PubMed]
5. Mak, K.F.; Lee, C.; Hone, J.; Shan, J.; Heinz, T.F. Atomically Thin MoS_2: A New Direct-Gap Semiconductor. *Phys. Rev. Lett.* **2010**, *105*, 136805. [CrossRef] [PubMed]
6. Radisavljevic, B.; Radenovic, A.; Brivio, J.; Giacometti, V.; Kis, A. Single-Layer MoS_2 Transistors. *Nat. Nanotechnol.* **2011**, *6*, 147–150. [CrossRef] [PubMed]
7. Li, L.; Yu, Y.; Ye, G.J.; Ge, Q.; Ou, X.; Wu, H.; Feng, D.; Chen, X.H.; Zhang, Y. Black Phosphorus Field-Effect Transistors. *Nat. Nanotechnol.* **2014**, *9*, 372–377. [CrossRef] [PubMed]
8. Novoselov, K.S.; Mishchenko, A.; Carvalho, A.; Castro Neto, A.H. 2D Materials and van Der Waals Heterostructures. *Science* **2016**, *353*, aac9439. [CrossRef] [PubMed]
9. Ortiz Balbuena, J.; Tutor De Ureta, P.; Rivera Ruiz, E.; Mellor Pita, S. Enfermedad de Vogt-Koyanagi-Harada. *Med. Clin.* **2016**, *146*, 93–94. [CrossRef]
10. Wse, L.; Allain, A.; Kis, A. Terms of Use Electron and Hole Mobilities in Single-layer WSe_2. *ACS Nano* **2014**, *8*, 7180–7185.

11. Pan, Y.; Jia, K.; Huang, K.; Wu, Z.; Bai, G.; Yu, J.; Zhang, Z.; Zhang, Q.; Yin, H. Near-Ideal Subthreshold Swing MoS 2 Back-Gate Transistors with an Optimized Ultrathin HfO_2 Dielectric Layer. *Nanotechnology* **2019**, *30*, 095202. [CrossRef] [PubMed]
12. Bolshakov, P.; Zhao, P.; Azcatl, A.; Hurley, P.K.; Wallace, R.M.; Young, C.D. Improvement in Top-Gate MoS_2 Transistor Performance Due to High Quality Backside Al_2O_3 Layer. *Appl. Phys. Lett.* **2017**, *111*, 032110. [CrossRef]
13. Lee, C.; Rathi, S.; Khan, M.A.; Lim, D.; Kim, Y.; Yun, S.J.; Youn, D.H.; Watanabe, K.; Taniguchi, T.; Kim, G.H. Comparison of Trapped Charges and Hysteresis Behavior in HBN Encapsulated Single MoS_2 Flake Based Field Effect Transistors on SiO_2 and HBN Substrates. *Nanotechnology* **2018**, *29*, 335202. [CrossRef] [PubMed]
14. Cassabois, G.; Valvin, P.; Gil, B. Hexagonal Boron Nitride Is an Indirect Bandgap Semiconductor. *Nat. Photonics* **2016**, *10*, 262–266. [CrossRef]
15. Geick, R.; Perry, C.H.; Rupprecht, G. Normal Modes in Hexagonal Boron Nitride. *Phys. Rev.* **1966**, *146*, 543–547. [CrossRef]
16. Illarionov, Y.Y.; Vexler, M.I.; Fedorov, V.V.; Suturin, S.M.; Sokolov, N.S. Electrical and Optical Characterization of Au/CaF_2/p-Si(111) Tunnel-Injection Diodes. *J. Appl. Phys.* **2014**, *115*, 223706. [CrossRef]
17. Usiskin, R.; Sigle, W.; Kelsch, M.; van Aken, P.A.; Maier, J. Ion Transport in Nanocrystalline CaF_2 Films. *J. Appl. Phys.* **2021**, *130*, 105301. [CrossRef]
18. Tyaginov, S.E.; Illarionov, Y.Y.; Vexler, M.I.; Bina, M.; Cervenka, J.; Franco, J.; Kaczer, B.; Grasser, T. Modeling of Deep-Submicron Silicon-Based MISFETs with Calcium Fluoride Dielectric. *J. Comput. Electron.* **2014**, *13*, 733–738. [CrossRef]
19. Illarionov, Y.Y.; Banshchikov, A.G.; Polyushkin, D.K.; Wachter, S.; Knobloch, T.; Thesberg, M.; Mennel, L.; Paur, M.; Stöger-Pollach, M.; Steiger-Thirsfeld, A.; et al. Ultrathin Calcium Fluoride Insulators for Two-Dimensional Field-Effect Transistors. *Nat. Electron.* **2019**, *2*, 230–235. [CrossRef]
20. Foster, A.S.; Trevethan, T.; Shluger, A.L. Structure and Diffusion of Intrinsic Defects, Adsorbed Hydrogen, and Water Molecules at the Surface of Alkali-Earth Fluorides Calculated Using Density Functional Theory. *Phys. Rev. B Condens. Matter Mater. Phys.* **2009**, *80*, 115421. [CrossRef]
21. Song, H.; Zhou, F.; Yan, S.; Su, X.; Wu, H.; Wu, Q.; Gao, Y.; Chen, R.; Chen, T.; Yao, J.; et al. Enhanced Transport and Optoelectronic Properties of van Der Waals Materials on CaF_2 Films. *Nano Lett.* **2023**, *23*, 4983–4990. [CrossRef] [PubMed]
22. Wen, C.; Banshchikov, A.G.; Illarionov, Y.Y.; Frammelsberger, W.; Knobloch, T.; Hui, F.; Sokolov, N.S.; Grasser, T.; Lanza, M. Dielectric Properties of Ultrathin CaF_2 Ionic Crystals. *Adv. Mater.* **2020**, *32*, e2002525. [CrossRef] [PubMed]
23. Huang, L.; Liu, H.; Cui, W. High-k Monolayer CaF_2 as the Gate Dielectric for Two-Dimensional SiC-Based Field-Effect Transistors. *ACS Appl. Electron. Mater.* **2023**, *5*, 5082–5092. [CrossRef]
24. Vishwanath, S.; Liu, X.; Rouvimov, S.; Mende, P.C.; Azcatl, A.; McDonnell, S.; Wallace, R.M.; Feenstra, R.M.; Furdyna, J.K.; Jena, D.; et al. Comprehensive Structural and Optical Characterization of MBE Grown $MoSe_2$ on Graphite, CaF_2 and Graphene. *2D Mater.* **2015**, *2*, 024007. [CrossRef]
25. Wen, C.; Lanza, M. Calcium Fluoride as High-k Dielectric for 2D Electronics. *Appl. Phys. Rev.* **2021**, *8*, 021307. [CrossRef]
26. Grasser, T.; Kaczer, B.; Goes, W.; Reisinger, H.; Aichinger, T.; Hehenberger, P.; Wagner, P.J.; Schanovsky, F.; Franco, J.; Toledano Luque, M.; et al. The Paradigm Shift in Understanding the Bias Temperature Instability: From Reaction-Diffusion to Switching Oxide Traps. *IEEE Trans. Electron Devices* **2011**, *58*, 3652–3666. [CrossRef]
27. Guo, Y.; Wei, X.; Shu, J.; Liu, B.; Yin, J.; Guan, C.; Han, Y.; Gao, S.; Chen, Q. Charge Trapping at the MoS_2-SiO_2 Interface and Its Effects on the Characteristics of MoS_2 Metal-Oxide-Semiconductor Field Effect Transistors. *Appl. Phys. Lett.* **2015**, *106*, 103109. [CrossRef]
28. Illarionov, Y.Y.; Waltl, M.; Bartolomeo, A.D.; Genovese, L.; Illarionov, Y.Y.; Rzepa, G.; Waltl, M.; Knobloch, T.; Grill, A. The Role of Charge Trapping in MoS_2/SiO_2 and MoS_2/HBN Field-Effect Transistors. *2D Mater.* **2016**, *3*, 035004. [CrossRef]
29. Di Bartolomeo, A.; Genovese, L.; Giubileo, F.; Iemmo, L.; Luongo, G.; Foller, T.; Schleberger, M. Hysteresis in the Transfer Characteristics of MoS_2 Transistors. *2D Mater.* **2018**, *5*, 015014. [CrossRef]
30. Late, D.J.; Liu, B.; Matte, H.S.S.R.; Dravid, V.P.; Rao, C.N.R. Hysteresis in Single-Layer MoS_2 Field Effect Transistors. *ACS Nano* **2012**, *6*, 5635–5641. [CrossRef]
31. Park, Y.; Baac, H.W.; Heo, J.; Yoo, G. Thermally Activated Trap Charges Responsible for Hysteresis in Multilayer MoS_2 Field-Effect Transistors. *Appl. Phys. Lett.* **2016**, *108*, 083102. [CrossRef]
32. Ma, X.; Liu, Y.Y.; Zeng, L.; Chen, J.; Wang, R.; Wang, L.W.; Wu, Y.; Jiang, X. Defects Induced Charge Trapping/Detrapping and Hysteresis Phenomenon in MoS_2 Field-Effect Transistors: Mechanism Revealed by Anharmonic Marcus Charge Transfer Theory. *ACS Appl. Mater. Interfaces* **2022**, *14*, 2185–2193. [CrossRef]
33. Xiong, T.; Yang, J.; Deng, H.-X.; Wei, Z.; Liu, Y.-Y. The Mechanism of Improving Germanium Metal–Oxide–Semiconductor Field-Effect Transistors' Reliability by High-k Dielectric and Yttrium-Doping: From the View of Charge Trapping. *J. Appl. Phys.* **2022**, *132*, 174506. [CrossRef]
34. Liu, Y.Y.; Liu, F.; Wang, R.; Luo, J.W.; Jiang, X.; Huang, R.; Li, S.S.; Wang, L.W. Characterizing the Charge Trapping across Crystalline and Amorphous Si/SiO2/HfO2 Stacks from First-Principle Calculations. *Phys. Rev. Appl.* **2019**, *12*, 064012. [CrossRef]
35. Liu, Y.Y.; Zheng, F.; Jiang, X.; Luo, J.W.; Li, S.S.; Wang, L.W. Ab Initio Investigation of Charge Trapping Across the Crystalline- Si -Amorphous- SiO_2 Interface. *Phys. Rev. Appl.* **2019**, *11*, 044058. [CrossRef]
36. Liu, Y.Y.; Jiang, X. Physics of Hole Trapping Process in High-k Gate Stacks: A Direct Simulation Formalism for the Whole Interface System Combining Density-Functional Theory and Marcus Theory. In Proceedings of the 2018 IEEE International Electron Devices Meeting (IEDM), San Francisco, CA, USA, 1–5 December 2018. [CrossRef]

37. Illarionov, Y.Y.; Knobloch, T.; Uzlu, B.; Banshchikov, A.G.; Ivanov, I.A.; Sverdlov, V.; Otto, M.; Stoll, S.L.; Vexler, M.I.; Waltl, M.; et al. Variability and High Temperature Reliability of Graphene Field-Effect Transistors with Thin Epitaxial CaF2 Insulators. *npj 2D Mater. Appl.* **2024**, *8*, 1–10. [CrossRef]
38. Durante, O.; Intonti, K.; Viscardi, L.; De Stefano, S.; Faella, E.; Kumar, A.; Pelella, A.; Romeo, F.; Giubileo, F.; Alghamdi, M.S.G.; et al. Subthreshold Current Suppression in ReS2 Nanosheet-Based Field-Effect Transistors at High Temperatures. *ACS Appl. Nano Mater.* **2023**, *6*, 21663–21670. [CrossRef] [PubMed]
39. Ishibe, T.; Tomeda, A.; Komatsubara, Y.; Kitaura, R.; Uenuma, M.; Uraoka, Y.; Yamashita, Y.; Nakamura, Y. Carrier and Phonon Transport Control by Domain Engineering for High-Performance Transparent Thin Film Thermoelectric Generator. *Appl. Phys. Lett.* **2021**, *118*, 151601. [CrossRef]
40. Xia, J.; Sohail, M.; Nazeeruddin, M.K. Efficient and Stable Perovskite Solar Cells by Tailoring of Interfaces. *Adv. Mater.* **2023**, *35*, e2211324. [CrossRef]
41. Li, Z.; Baskurt, M.; Sahin, H.; Gao, S.; Kang, J. Electronic Properties of Intrinsic Vacancies in Single-Layer CaF_2 and Its Heterostructure with Monolayer MoS_2. *J. Appl. Phys.* **2021**, *130*, 055301. [CrossRef]
42. Zhang, H.; Shi, B.; Xu, L.; Yan, J.; Zhao, W.; Zhang, Z.; Zhang, Z.; Lu, J. Sub-5 Nm Monolayer MoS_2 Transistors toward Low-Power Devices. *ACS Appl. Electron. Mater.* **2021**, *3*, 1560–1571. [CrossRef]
43. Hua, Q.; Gao, G.; Jiang, C.; Yu, J.; Sun, J.; Zhang, T.; Gao, B.; Cheng, W.; Liang, R.; Qian, H.; et al. Atomic Threshold-Switching Enabled MoS_2 Transistors towards Ultralow-Power Electronics. *Nat. Commun.* **2020**, *11*, 6207. [CrossRef] [PubMed]
44. Huang, B.; Li, N.; Wang, Q.; Ouyang, C.; He, C.; Zhang, L.; Du, L.; Yang, W.; Yang, R.; Shi, D.; et al. Optoelectronic Synapses Based on MoS_2 Transistors for Accurate Image Recognition. *Adv. Mater. Interfaces* **2022**, *9*, 2201558. [CrossRef]
45. Di Bartolomeo, A.; Kumar, A.; Durante, O.; Sessa, A.; Faella, E.; Viscardi, L.; Intonti, K.; Giubileo, F.; Martucciello, N.; Romano, P.; et al. Temperature-Dependent Photoconductivity in Two-Dimensional MoS_2 Transistors. *Mater. Today Nano* **2023**, *24*, 100382. [CrossRef]
46. Hong, Y.L.; Liu, Z.; Wang, L.; Zhou, T.; Ma, W.; Xu, C.; Feng, S.; Chen, L.; Chen, M.L.; Sun, D.M.; et al. Chemical Vapor Deposition of Layered Two-Dimensional $MoSi_2N_4$ Materials. *Science* **2020**, *369*, 670–674. [CrossRef] [PubMed]
47. Zhao, P.; Jiang, Z.Y.; Zheng, J.M.; Lin, Y.M.; Du, A. Theoretical Study of a Novel $WSi_2N_4/MoSi_2N_4$ Heterostructure with Ultrafast Carrier Transport. *J. Phys. Chem. C* **2022**, *126*, 11380–11388. [CrossRef]
48. Mortazavi, B.; Javvaji, B.; Shojaei, F.; Rabczuk, T.; Shapeev, A.V.; Zhuang, X. Exceptional Piezoelectricity, High Thermal Conductivity and Stiffness and Promising Photocatalysis in Two-Dimensional $MoSi_2N_4$ Family Confirmed by First-Principles. *Nano Energy* **2021**, *82*, 105716. [CrossRef]
49. Yang, J.-S.; Zhao, L.; LI, S.-Q.; Liu, H.; Wang, L.; Chen, M.; Gao, J.; Zhao, J. Accurate Electronic Properties and Non-Linear Optical Response of Two-Dimensional MA_2Z_4. *Nanoscale* **2021**, *13*, 5479–5488. [CrossRef]
50. Jia, W.; Fu, J.; Cao, Z.; Wang, L.; Chi, X.; Gao, W.; Wang, L.W. Fast Plane Wave Density Functional Theory Molecular Dynamics Calculations on Multi-GPU Machines. *J. Comput. Phys.* **2013**, *251*, 102–115. [CrossRef]
51. Jia, W.; Cao, Z.; Wang, L.; Fu, J.; Chi, X.; Gao, W.; Wang, L.W. The Analysis of a Plane Wave Pseudopotential Density Functional Theory Code on a GPU Machine. *Comput. Phys. Commun.* **2013**, *184*, 9–18. [CrossRef]
52. Hamann, D.R. Optimized Norm-Conserving Vanderbilt Pseudopotentials. *Phys. Rev. B Condens. Matter Mater. Phys.* **2013**, *88*, 085117. [CrossRef]
53. Heyd, J.; Peralta, J.E.; Scuseria, G.E.; Martin, R.L. Energy Band Gaps and Lattice Parameters Evaluated with the Heyd-Scuseria-Ernzerhof Screened Hybrid Functional. *J. Chem. Phys.* **2005**, *123*, 174101. [CrossRef] [PubMed]
54. Grimme, S.; Antony, J.; Ehrlich, S.; Krieg, H. A Consistent and Accurate Ab Initio Parametrization of Density Functional Dispersion Correction (DFT-D) for the 94 Elements H-Pu. *J. Chem. Phys.* **2010**, *132*, 154104–154119. [CrossRef] [PubMed]
55. Chen, J.; Zhang, Z.; Guo, Y.; Robertson, J. Electronic Properties of CaF_2 bulk and Interfaces. *J. Appl. Phys.* **2022**, *131*, 215302. [CrossRef]
56. Zhou, W.; Zou, X.; Najmaei, S.; Liu, Z.; Shi, Y.; Kong, J.; Lou, J.; Ajayan, P.M.; Yakobson, B.I.; Idrobo, J.C. Intrinsic Structural Defects in Monolayer Molybdenum Disulfide. *Nano Lett.* **2013**, *13*, 2615–2622. [CrossRef] [PubMed]
57. Robertson, J.; Falabretti, B. Band Offsets of High K Gate Oxides on III-V Semiconductors. *J. Appl. Phys.* **2006**, *100*, 014111. [CrossRef]
58. Robertson, J. Band Offsets, Schottky Barrier Heights, and Their Effects on Electronic Devices. *J. Vac. Sci. Technol. A Vacuum Surfaces Film.* **2013**, *31*, 050821. [CrossRef]
59. Robertson, J. Band Offsets of Wide-Band-Gap Oxides and Implications for Future Electronic Devices. *J. Vac. Sci. Technol. B Microelectron. Nanometer Struct.* **2000**, *18*, 1785. [CrossRef]